Research Square

Preprints are preliminary reports that have not undergone peer review.
They should not be considered conclusive, used to inform clinical practice,
or referenced by the media as validated information.

Cyclic Soft/Hardening and Microscopic Mechanism of GS-20Mn5

Zongyuan Zou (zzy@ysu.edu.cn)
Yanshan University
Doudou Liu
Yanshan University
Shuting Han
Yanshan University
Chunyan Song
Yanshan University
Hongzhong Wang
Yanshan University

Research Article

Keywords: GS-20 Mn5 steel, Strain control, Cyclic loading, Cyclic softening/hardening, dislocation

Posted Date: July 8th, 2021

DOI: https://doi.org/10.21203/rs.3.rs-654341/v1

License: This work is licensed under a Creative Commons Attribution 4.0 International License.
Read Full License

Abstract

The cyclic plastic characteristics of metal materials are different from the deformation characteristics under monotonic loading, which has an important effect on the safety of structures in service under cyclic loading. However, GS-20Mn5, which is commonly used in large hydraulic machine beams, offshore platforms and large Bridges, is still lacking the studies of mechanical response characteristics under cyclic loading. In this study, the cyclic softening/hardening characteristics of GS-20Mn5 are studied by a series of cyclic loading tests under uniaxial strain control. Combined with transmission electron microscope (TEM) analysis of cyclic loading tests under typical strain levels, the microscopic mechanism of cyclic softening/hardening is discussed. The results show that the cyclic softening/hardening properties of GS-20Mn5 cast steel are sensitive to amplitudes and cycles. At smaller strain amplitudes (0.16%,0.2% and 0.3%), the cyclic hardening properties of GS-20Mn5 cast steel are rapid at the beginning of the cycle, followed by cyclic softening and then slow secondary cyclic hardening at the end. However, under larger strain amplitudes (0.4% and 0.5%), the cyclic hardening continues during the cyclic loading, and the hardening rate is bigger at the beginning of the cyclic loading and smaller at the later cyclic stage. The cyclic softening/hardening characteristics of GS-20Mn5 cast steel are related to the dislocation structure of ferrite and pearlite. Taking the strain amplitude of 0.2% as an example, the initial cyclic hardening is mainly caused by the proliferation and interaction of dislocations in ferrite. Dislocation spots and cell walls in ferrite grains are mainly caused cyclic softening at the initial stage, the secondary cyclic hardening is directly related to dislocation proliferation and entanglement in pearlite.

1 Introduction

GS-20Mn5 cast steel is widely used in hydraulic press beam worktables, large-span building steel structures, bridges and offshore platform steel structures because their high strength and good plasticity [1]. Therefore, the research mainly focuses on uniaxial tensile mechanical properties, welding process [1-2]and chemical composition optimization of GS-20Mn5 cast steel [3-4]. Mechanical properties are rarely studied under cyclic loading. During the actual service process, metal structure is usually subjected to the cyclic loading, the mechanical properties of metal materials under the cyclic loading is different from that under the monotonic loading. The metal material obviously occurs cyclic hardening, cyclic softening or cyclic stability, which are important characteristics of cyclic deformation responses and play important roles in the service safety of the structure under cyclic loading conditions [5-7].

Due to the important influence of cyclic response characteristics of metal materials on the bearing safety of structures, the cyclic response characteristics of metals have been studied extensively. Li Fei et al, carried out cyclic loading test of Mn18Cr18N steel under strain amplitudes of 0.005-0.15 at room temperature, found that the cumulative plastic strain could improve the strength of the steel, because the cyclic hardening of metal material under the cyclic loading [8]. Kosuge Hiroaki had studied the variation of brittle fracture toughness of three different ferrite/pearlite two-phase steels under cyclic pre-strain loading, which revealed that material damage due to brittle fracture can be evaluated by using the

effective damage strain with back stress updating proposed by Ohata et al [9]. Atri Nath studied the symmetrical strain cyclic response of low carbon steel YST210 under different strain amplitudes and strain rates, and described cyclic characteristics of the low carbon steel YST210 to establish a Bilinear Kinemat hardening model [10]. Zhiyang Xie studied the cyclic characteristics of Q345 steel plate and established the cyclic plastic constitutive model [11]. Caina Bemfica studied the evolution of the backstress limit of surface size and the volume fraction of martensite in metastable austenitic stainless steel under cyclic loading, established the secondary hardening model of metastable stainless steel with strain-induced martensitic transformation [12]. These studies provide important theoretical support for understanding the cyclic response characteristics of metal materials and establishing corresponding cyclic constitutive models for numerical analysis, as well as can provide a powerful reference for the studies of other metal materials.

Previous studies have also shown that the cyclic characteristics are closely related to the evolution of microstructure. In order to further study and understand the cyclic characteristics of metal materials, the microscopic mechanism of cyclic response characteristics has gradually attracted the attention of scholars. For metallic polycrystalline materials, the cyclic plastic deformation behavior is mainly related to the evolution of microstructure, such as the proliferation, annihilation and rearrangement of dislocations [13]. Petrenec M et al. [14] studied the dislocation structure of ferritic stainless steel under the low cyclic fatigue, pointed out that the dislocation structure is vein and wall structure under the lower strain amplitude. And the dislocation structure is maze and cell structures under the higher strain amplitude. Shuto H et al. [15] studied the causes of the formation of dislocation walls, found that the dislocation slides along a single slip surface at the initial stage of deformation, the activation of other slip systems leads to the "wall" shape of the dislocation structure. Tsai Y T et al [16] studied the fatigue behavior and dislocation structure of SAF2507 alloy, found that the alloy is hardened firstly and then softened under the cyclic loading. The vein structures are found in the fatigue ferrite sample, and the dislocation walls and dislocation cell structures are found in the grain, which is directly related to the cyclic softening/hardening. The evolution of dislocation from dislocation entanglement to dislocation cell obviously affects the change of grain structures of the material, which leads to the softening/hardening characteristics of the material at different stages with the increase of deformation degree. G.I. Reab [17] analyzed the relationship between the strain hardening characteristics and microstructure evolution of ferritic-pearlite steel, found that the hardening characteristics are determined by the dislocation structure formed at coincident stage of deformation. It can be seen that the evolution of dislocation structure is the microscopic mechanism that plays an important role in the softening/hardening properties of metals under the cyclic loading.

The GS-20Mn5 steel is widely used in steel structures [18], but the cyclic softening/hardening characteristics and microscopic mechanism are rarely reported [19]. In this study, the cyclic loading response characteristics of GS-20Mn5 steel at a series of strain levels were studied and the microstructure evolution was analyzed to reveal the cyclic softening/hardening characteristics and the

micro-mechanism of GS-20Mn5 steel, which provide necessary reference for the design of analysis and service performance evaluation of GS-20Mn5 cast steel.

2 Specimen And Method

2.1 Experimental material

The GS-20Mn5 steel used in the experiment is observed and analyzed after being tempered and reduced to room temperature. The specific chemical composition is shown in Table 1. The metallographic image of the origin structure is shown in Fig.1, and the white portion is ferrite and the black one is pearlite.

2.2 Monotonic tensile test

The circular cross-section sample is designed by the method of ASTME345-2016 standard, as shown in Fig. 2. The diameter of the gauge section is 5mm, and the length of the gauge section is 25mm.The monotonic tensile test was carried out with Instron 100kN (Instron 8801) series servohydraulic testing machine at room temperature. The strain was measured by contact extensometer. The loading rate is 0.1%/s. Three repeated tensile tests were carried out.

2.3 Cyclic loading test

The cyclic loading sample is designed by the tensile test method of the ASTM E606 standard at room temperature [20], as shown in Fig. 3. The diameter of gauge length section is 5mm, the length of gauge length section is 12.5mm, and the length of parallel section is 15mm.

The cyclic loading tests controlled was carried out by Instron 100KN machine at room temperature. The strain control was adopted, and the loading rate was 0.2% per second, and the strain amplitudes were 0.16%, 0.2%, 0.3%, 0.4% and 0.5%, respectively. The strain amplitudes of 0.16%, 0.2% and 0.3% were loaded for 3000 cycles and the strain amplitudes of 0.4% and 0.5% were loaded to fatigue failure. The strain amplitude of 0.4% was loaded for 2454 cycles, and the strain amplitude of 0.5% was loaded for 1811 cycles. The test scheme is shown in Table 2, and the experimental photos are shown in Figure 4.

In addition, according to the cyclic response results obtained from the test, it is proposed to select 0.2% characteristic strain amplitude to carried out the cyclic loading test under different cycles. The test scheme is shown in Table 3, In order to study the microstructural evolution law of the test steel under cyclic loading.

The microstructural characteristic of the samples was observed by transmission electron microscope (TEM). The samples were cut along the loading axis within the sample gauged section and polish thickness to 20-50μm, and then the samples are thinned at room temperature using the Tenupol-5 electrolytic double spray. The electrolyte is perchloric by acid alcohol solution with 7.5% volume fraction, the voltage is set to 26V, the sensitivity is set to 66, and the flow rate is set to 18. TEM analysis was performed on JEM-2010 transmission electron microscope, and the operating voltage was 20kV.

3 Experimental Results And Analysis

3.1 Stress-strain curve

The monotonic tensile stress-strain curve and cyclic stress-strain curve of GS-20Mn5 used in this test are shown in Fig. 5.

The results show that GS-20Mn5 has an obvious yield platform under monotonic tensile process. The strain range of the platform section is about 0.00156 ~ 0.0099, the yield limit is 310MPa, the tensile strength is 542MPa and the elastic modulus is 212GPa.

The cyclic stress-strain curve in Fig. 5 is formed by connecting the stress amplitudes of cyclic stability under different strain amplitudes, which reflects the mechanical properties of the material under cyclic loading. Due to cyclic softening/hardening, it can be seen from the figure that the cyclic stress-strain curve of the sample steel does not coincide with the uniaxial tensile stress-strain curve, according to the curve, the strain at the intersection is about 0.3%. That is to say, when the strain is less than 0.3%, the test steel shows cyclic softening characteristics; When the strain is higher than 0.3%, it shows cyclic hardening.

3.2 Cyclic soft/ hardening characteristics

Hysteresis loops with strain amplitudes of 0.16%, 0.20%, 0.30%, 0.40% and 0.50% are obtained according to the experiment. The hysteresis loops of typical cycle amplitude with strain amplitudes of 0.16%, 0.20%, 0.30%, 0.40% and 0.50% are presented here, as shown in Fig.6. The hysteretic loops of the stable cycle under various strain amplitudes are shown in Fig. 7.

It can be seen from Fig. 6 that the cyclic stress-strain hysteresis loops of GS-20Mn5 materials are different under different strain amplitudes. As the increase of cycles, the shape and the peak-valley value of the hysteresis loop will change. Under the strain amplitudes of 0.16%,0.2% and 0.3%, the hysteresis loop first becomes sharp, and the peak and valley of stress increase gradually, which shows the initial cyclic hardening. Then the hysteresis loop became flat, the peak and valley of stress decrease gradually, which shows the cyclic softening. Then it changes from flat to sharp, the peak and valley of stress increase gradually, it occurs cyclic hardening again (secondary cyclic hardening). Under the strain amplitudes of 0.4% and 0.5%, the cyclic hysteresis loop gradually becomes sharp, the peak and valley of stress gradually increase, which always shows cyclic hardening. It can be seen from Fig. 7, under low strain amplitude, the loop is slender and sharp. With the increase of strain amplitude, the loop becomes wider, while the peak and valley of stress increase and gradually flatten out.

The variation curve of stress amplitude of test steel under different strain amplitudes with cycles is shown in Fig. 8. It can be seen from the figure that the cyclic softening/hardening characteristics of the test steel are sensitive to amplitude variation and cycles. When the strain amplitudes are 0.16%, 0.2% and 0.3%, the stress amplitude increases gradually at the initial cyclic stage, showing slow cyclic hardening. Then the stress amplitude gradually decreased with the cycles, showing cyclic softening; The subsequent

stress amplitude gradually increases, which showing cyclic hardening, i.e., the secondary cyclic hardening. The larger the strain amplitude is, the shorter the cyclic softening stage is and the higher the softening rate is. When the strain amplitude is 0.4% and 0.5%, the stress amplitude increases rapidly at the beginning of the cycles (2-10 cycles), showing rapid hardening followed by slow hardening(1-2cycles) and there is no cyclic softening phenomenon in the whole cyclic loading.

3.3 Evolution of microstructures

The steel samples with strain amplitude of 0.2% showed obvious initial cyclic hardening, the subsequent cyclic softening, and occur secondary cyclic hardening at last, the loop softening/hardening characteristics change significantly, therefore, choose the strain amplitude cyclic loading tests of different cycles. The steel cyclic softening/hardening characteristic of microscopic mechanisms is analyzed through microstructure observation and analysis. In addition, microscopic observations are also made for samples with strain amplitudes of 0.16%, 0.3% lower cycle for 3000 cycles, and 0.4% lower cycle for 2450 cycles, respectively.

Fig. 9 shows the dislocation structure of the original sample. Fig. 9 (a) shows the dislocation structure of ferrite. From which it can be concluded that some short-range dislocation lines are mainly scattered and generated in the heat treatment process of the test steel. Fig. 9 (b) shows the dislocation structure in pearlite, which the fine-rod-shaped pearlite is lamellar. And some spherical pearlites can be observed between the lamellar pearlites, some short-range dislocation structures can be also observed in the cracks between pearlites.

Figure 10 shows dislocation structure at the strain amplitude of 0.2% under 10 cycles corresponding to the stage of cyclic hardening. Dislocations occur at the grain boundaries. The initiation of dislocations and the interaction between dislocations make the pearlite/ferrite interface has a very high dislocation density, and entangle each other. Fig. 10 (a) shows the dislocations at the boundary of ferritic grains. Due to the discordant intergranular deformation, grain boundary will act as a source of dislocation then continuously insert dislocations in the grain, which makes the material develop towards hardening. Fig. 10 (b) shows the situation of cementite pinning dislocation inside ferrite grains. The pinning effect of cementite on dislocation hinds dislocation movement, which increases the deformation resistance of the material and makes the material develop towards hardening. Figure 10 (c) shows the dislocation stacking at the ferrite grain boundaries. Since the ferrite grain boundary obstructs the dislocation movement, the dislocation stacking occurs here and there is a reverse force on the dislocation source. Consequently, it needs a larger shear force to make the dislocation move which causes the hardening of the material. Fig. 10 (d) shows the high-density dislocation entanglements in ferrite grains. These dislocation entanglements hinder dislocation movement and cause the material to develop towards hardening. At this stage, the dislocation accumulation at the grain boundary of ferrite and the cementite pin in the grain lead to the hardening of the material. Since the dislocation characteristics of pearlite at this stage are not significantly different from that at the initial state, it has little hardening effect on the material.

After cyclic deformation under 60 cycles at a strain range of 0.2%, The steel samples with strain amplitude of 0.2% showed obviously cyclic softening. The dislocation structure is shown in Fig. 11. Dislocation annihilation occurs in ferrite grains. Fig. 11 (a) shows dislocation walls and dislocation spots begin to form. However, at the transformation stage, the dislocation arrangement is still disorder. On the one hand, dislocation structure form in ferrite that make high stacking fault energy, so under the action of dislocation interaction, the dislocation of multiple sliding systems start repeatedly positive and reverse slip, some different direction dislocations offset each other during movement process lead to the dislocation annihilation. Eventually, the movement leads to the decrease of the dislocation density then dislocation slip resistance decreases and the materials softening occur; On the other hand, because of the dislocation mechanism of pinning, the dislocations pinned by carbides in the dislocation spots are dislocated during cyclic deformation, which resulting in the decrease of friction stress. Consequently, dislocation entanglement and grain boundaries are also destroyed under cyclic loading, which makes dislocation disorder and distributed in the shape of network. It enhances the mobility of dislocations, which lead to the softening of the material. As shown in figure 11 (b) and (c), the pearlite lamellar have the same orientation at the initial stage. And the dislocation sources at the pearlite interface continuously emit dislocations outwards after deformation. The dislocations begin to accumulate, which expands into ferrite in the form of dislocation rings and gradually forms dislocation walls. But it began to form dislocation lines across ferrite and pearlite when the dislocation loop front-end and adjacent pearlite lamellar intersect. In the dislocation wall as shown in Fig.11 (c), lamellar pearlite ruptures and dislocation annihilation at the fracture, which leads to softening [21]. At this stage, the offset of hetero-sign dislocations in ferrite grains, the mechanism of dislocation pinning and the annihilation of lamellar dislocation in pearlite grains all lead to the cyclic softening of the materials.

Fig. 12 shows the dislocation structure with 3000 cycles at strain amplitude of 0.2%, which corresponds to the secondary cyclic hardening stage. Compared with the dislocation structure of the 60 cycles, the dislocation structure in ferrite grains during this period is mainly mature dislocation walls, as shown in Fig. 12 (a). This dislocation structure is in a stable state and has little influence on the softening/hardening properties of the material. It can be seen from Fig. 12 (b) that there are many dislocation lines between the lamellar pearlite. These entanglements in the pearlite hinder the movement of the dislocation. The deformation resistance increase which leads to obvious cyclic hardening of the material. So the secondary hardening is directly related to the dislocation in the pearlescent body.

In summary, at the early cyclic stage, the dislocation accumulation at the ferrite grain boundary and the dislocation tangle in the grain dominate the hardening characteristics of the material; in the subsequent cycles, the dislocation in the ferrite annihilates and gradually forms the dislocation walls, which dominates the softening characteristics of the material; at the late cyclic stage, the dislocation of the pearlite begins to entangle in the grain, which prompts the material to present the hardening characteristics again.

The dislocation structures in ferrite with strain amplitudes of 0.16%, 0.3%, and 0.4% for about 3000 cycles are shown in Figure 13. When the strain amplitude is 0.16%, the dislocation structure is mainly the

dislocation "spot" with higher dislocation density, and there is a channel with lower dislocation density between the dislocation "spot"; when the strain amplitude is 0.2%, the dislocation structure in the ferrite is mainly the parallel wall (shown in Figure 12 a); when the strain amplitude is 0.3%, there is also the dislocation wall structure, but the dislocation wall is mainly wavy, there are a large number of dislocations between the walls which cut the dislocation walls, and a small number of dislocation walls have been surrounded by cellar structures; when the strain amplitude is 0.4%, a large number of dislocation cells (substructures) are generated. It has been shown that during the deformation of the material [22-24], the change process of dislocation structure inside the grain is: dislocation tangle - dislocation spot - dislocation wall - immature dislocation cell - mature dislocation cell. It can be seen that with the increase of strain amplitude, the test steel is more likely to form dislocation walls and more stable dislocation structures. Different dislocation structures dominate the cyclic softening/hardening characteristics of each stage of the material at different cycles under different strain amplitudes.

4 Conclusion

(1) Compared with the monotonic tensile curve, the cyclic stress-strain curve of GS20Mn5 steel shows that the sample steel presents cyclic softening when the strain amplitude is less than 0.32%; while when the strain amplitude is greater than 0.32%, the test steel shows cyclic hardening.

(2) The cyclic softening and hardening characteristics of GS20Mn5 steel are sensitive to strain amplitude and cycles. At small strain amplitudes (0.16%, 0.2%, 0.3%), cyclic hardening is present initially, followed by cyclic softening, and finally by secondary cyclic hardening. Under larger strain amplitudes (0.4%, 0.5%), it shows continuous cyclic hardening during the cycles, and the hardening rate is bigger at the early cyclic stage and smaller at the late cyclic stage.

(3) The cyclic soft/hardening properties of GS20Mn5 steel are closely related to the dislocation structure evolution of each phase. At 0.2% strain amplitude, due to the hindrance of ferrite grain boundary, carbide pinning and entanglement between dislocations in the initial cyclic stage the movement of dislocations are hindered, resulting in cyclic hardening characteristics of the material. In the cyclic softening stage, the dislocation evolution in the ferrite dominates the cyclic softening of the material, on the one hand, the dislocation wall is formed in the ferrite, and the heterochromatic dislocations cancel each other, which decreases the dislocation density; on the other hand, due to the nailing mechanism of the dislocation in the ferrite dislocation spot, the mobility of the dislocation is improved; the pearlite lamellae produce dislocation accumulation at this stage, the lamellar pearlite breaks, and the dislocation annihilates at the breaks, resulting in softening. In the second cyclic hardening stage, the dislocations in ferrite are mainly stable dislocation cells, which have little effect on the cyclic softening/hardening performance. The entanglement of dislocations in pearlite is the main reason for the secondary cyclic hardening of materials.

References

1. Haidong Wang, Jinwen Ju, Jianchun Wang. Welding Process of 90mm Steel Casting GS-20Mn5+E Grade Steel [J]. Ship Standardization Engineer, 2013, 46(4):34-36.
2. Sun Kaimin, Jia Baohua. Welding of Q460E-Z35 and GS20Mn5V Dissimilar Steel. Electric Welding Machine, 2012, 42(8):20-25.
3. Peruš Iztok,Palkowski Heinz,Kugler Goran,Terčelj Milan. Quantifying complex influences of chemical composition and soaking conditions for increasing the hot workability of M2 high-speed steel by using the alternative approach[J]. Journal of Materials Research and Technology,2020,9(6).
4. Svobodová Jaroslava,Michna Štefan,Hren Iryna. Fractographic Analysis of Castings from Al-Si Alloy Produced by Low-Pressure Casting[J]. Materials Science Forum,2020,6102.
5. Strubbia R, Marinelli M C, et al. Fatigue damage in coarse-grained lean duplex stainless steels[J]. Materials Science and Engineering: A, 2016, 659:47-54
6. J.R.O. Leo,S.R. Moturu,M.E. Fitzpatrick. TEM study of the effect of high-temperature thermal cycles on the stability of the Y-Al-O oxides in MA956 ODS steel[J]. Journal of Materials Research and Technology,2019,8(5).
7. Paul S K, Stanford N, Taylor A, et al. The effect of low cycle fatigue, ratcheting and mean stress relaxation on stress-strain response and microstructural development in a dual phase steel[J]. International Journal of Fatigue, 2015, 80(nov.):341-348.
8. Fei Li,Huayu Zhang,Wenwu He,Xiaodong Zhao,Huiqin Chen. Stress softening and hardening during compression and tensile consecutive cyclic loading of Mn18Cr18N austenitic stainless steel[J]. Materials Science & Engineering A,2017,704.
9. Kosuge Hiroaki,Kawabata Tomoya,Okawa Teppei. Microstructural design strategy to maintain the brittle fracture toughness of hard-soft dual phase steel after cyclic plastic strain[J]. Materials & Design,2021,203.
10. Nath Atri,Barai Sudhirkumar V.,Ray Kalyan Kumar. Studies on the experimental and simulated cyclic-plastic response of structural mild steels[J]. Journal of Constructional Steel Research,2021,182.
11. Xie Zhiyang,Chen Yiyi. Experimental and modeling study of cyclic plasticity and ductile fracture of thin structural steel sheets[J]. Thin-Walled Structures,2021,162.
12. Bemfica Cainã,Castro Fábio. A cyclic plasticity model for secondary hardening due to strain-induced martensitic transformation[J]. International Journal of Plasticity,2021(prepublish).
13. Fei Li, Huayu Zhang, Wenwu He, Huiqin Chen, Huiguang Chen.Deformation Behavior of Mn18Cr18N Austenitic Stainless Steel under Continuous Compression and Tensile Loading [J]. Acta Metall Sin,2016,52(08):956-964.
14. Petrenec M, J. Polák, K. Obrtlík, et al. Dislocation structures in cyclically strained X10CrAl24 ferritic steel[J]. Acta Materialia, 2006, 54(13):3429-3443.
15. Shuto H, Tanaka Y, Miyazawa T, et al. Formation Mechanism of Dislocation Walls during Cyclic Deformation in an Fe–Si Alloy[J]. Isij International, 2019

16. Yu-Ting Tsai,Po-Chiang Lin,Yu-Wen Chen,Shing-Hoa Wang,Jer-Ren Yang. Fatigue behavior and microstructural characteristics of a duplex stainless steel weld metal under vibration-assisted welding[J]. Materials Science & Engineering A,2018,721.
17. Raab G I, Podrezov Y M, Aleshin G N. Dislocation Structure Evolution during Plastic Deformation of Low-Carbon Steel[J]. Materials Science Forum, 2016, 870:253-258
18. DIN EN 10293 (2005). Steel castings for general engineering uses. European Committee for Standardization (CEN), Brussels, Belgium.
19. Han Q, Guo Q, Yin Y, et al. Fatigue Behaviour of G20Mn5QT Cast Steel and Butt Welds with Q345B Steel[J]. International Journal of Steel Structures, 2016, 16(1):139-149.
20. GB/T 228.1-2010, Tensile testing of metallic materials -- Part 1: Test method at room temperature [S].
21. Tian-Zhang Zhao,Shi-Hong Zhang,Guang-Liang Zhang,Hong-Wu Song,Ming Cheng. Hardening and softening mechanisms of pearlitic steel wire under torsion[J]. Materials and Design,2014,59.
22. Jianfeng Zhang, Fuzhen Xun. Nonlinear Ultrasonic Evaluation of Fatigue Damage and Ratchet Damage in Austenitic Steel Vessel [J]. China Special Equipment Safety,2015,31(S1):17-25.
23. Sergio Neves Monteiro,Lucio Fabio Cassiano Nascimento,Noan Tonini Simonassi,Eduardo Sousa Lima,Andersan Santos de Paula,Fabio de Oliveira Braga. High temperature work hardening stages, dynamic strain aging and related dislocation structure in tensile deformed AISI 301 stainless steel [J]. Journal of Materials Research and Technology,2018.
24. Das A. Cyclic plasticity induced transformation of austenitic stainless steels[J]. Materials Characterization, 2019: 1-25.

Tables

Due to technical limitations, table 1-3 is only available as a download in the Supplemental Files section.

Figures

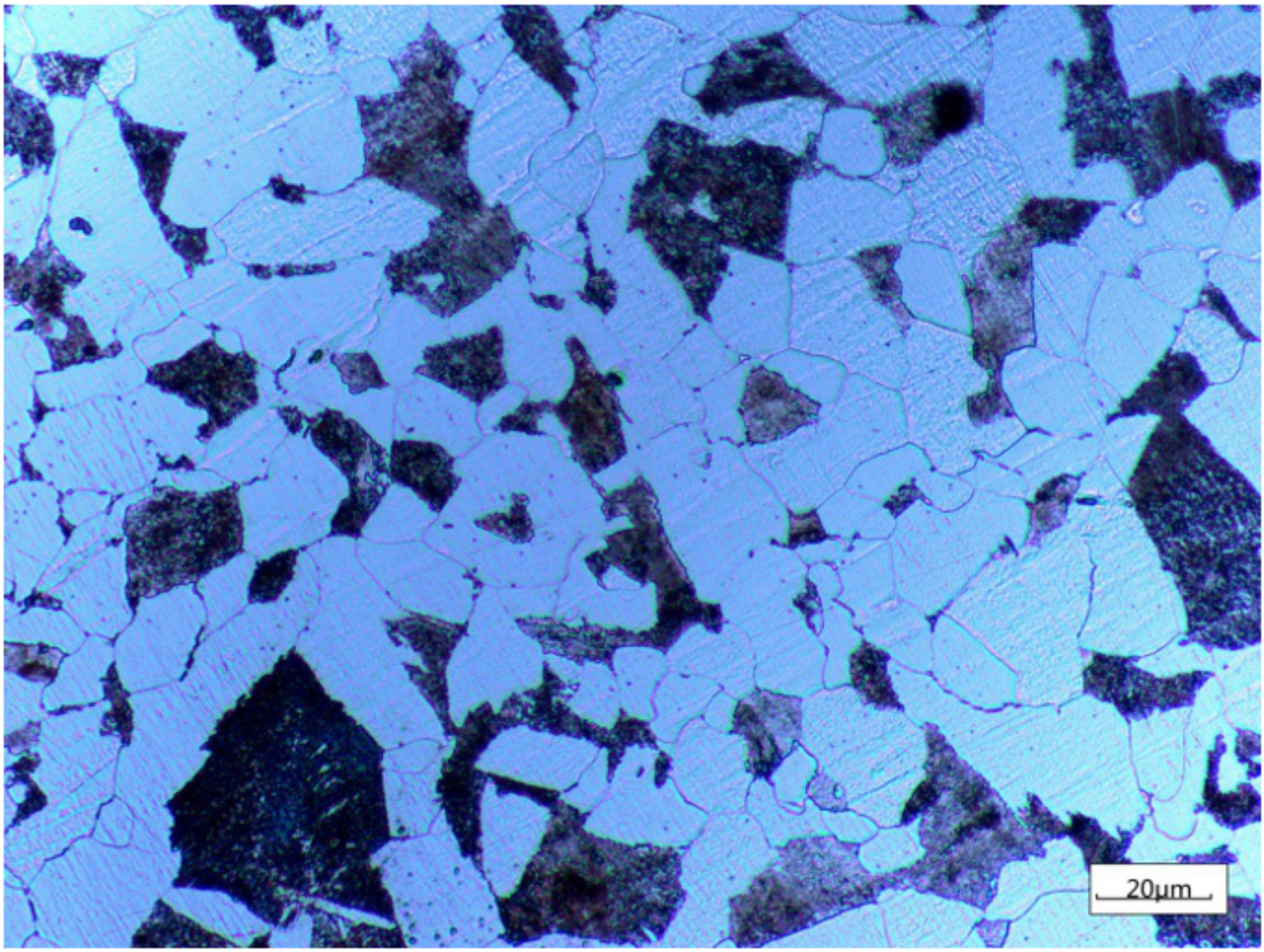

Figure 1

Metallographic image of GS-20Mn5 cast steel

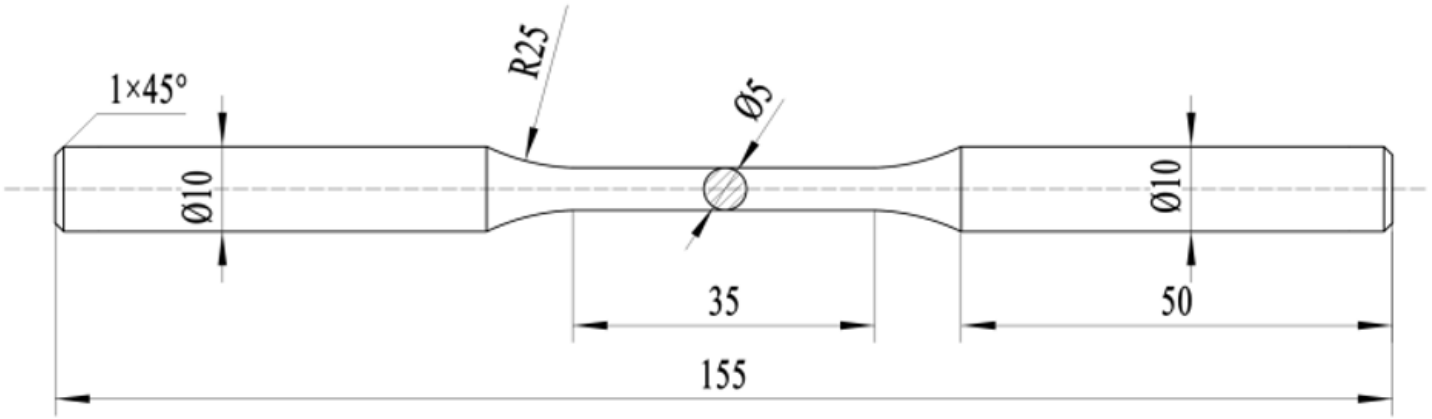

Figure 2

Dimensions of monotonic tensile specimen

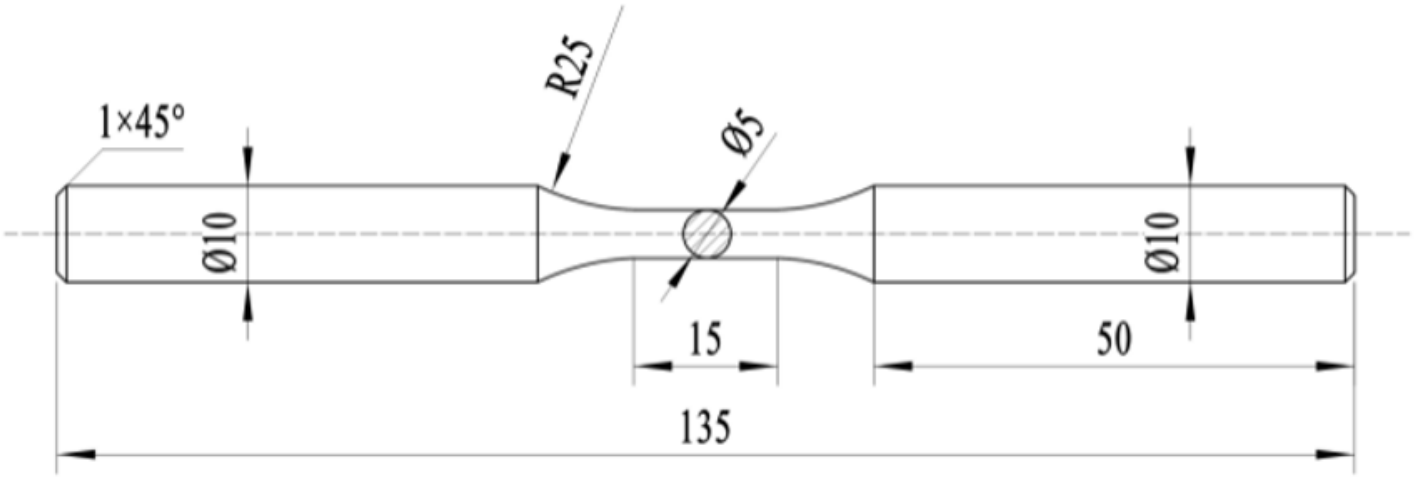

Figure 3

Schematic diagram of sample size under cyclic loading

Figure 4

Site photos of cyclic loading test

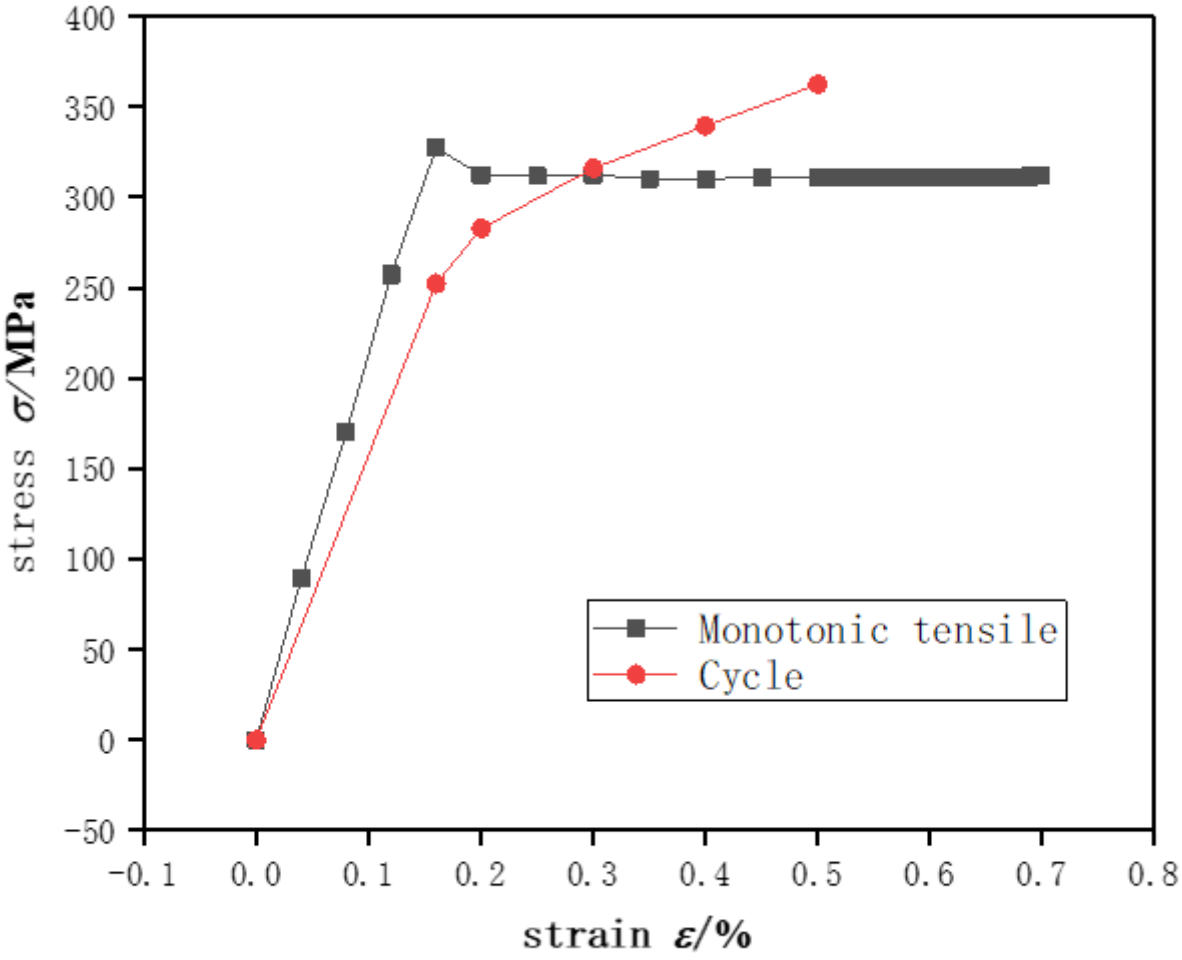

Figure 5

Monotonic tension and cyclic stress-strain curves

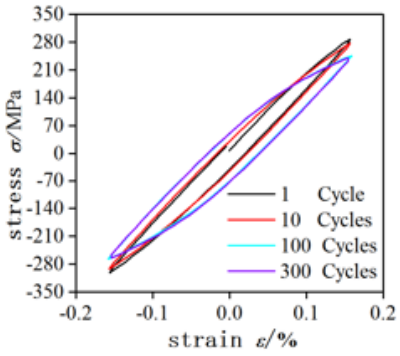

（a）Strain amplitude 0.16%

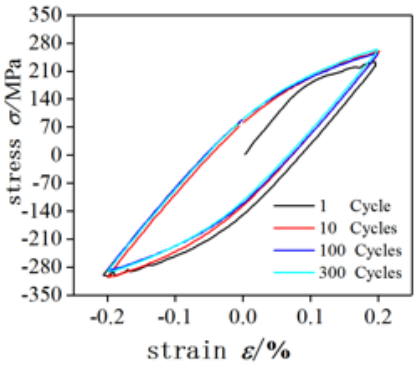

（b）Strain amplitude 0.20%

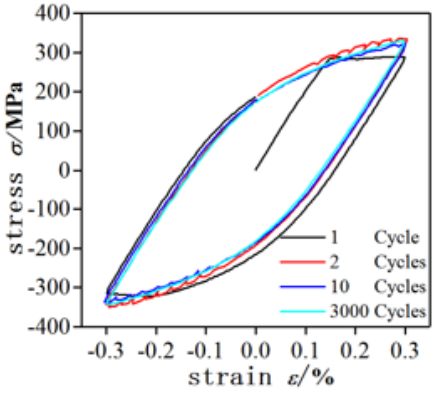

（c）Strain amplitude 0.30%

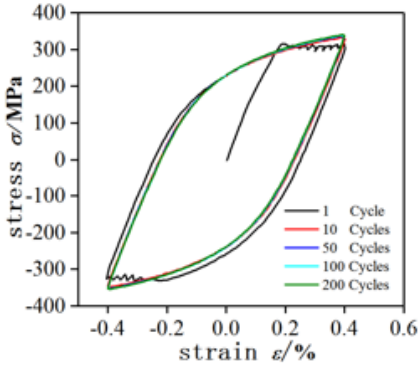

（d）Strain amplitude 0.40%

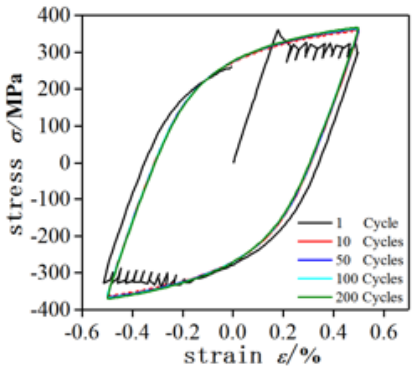

（e）Strain amplitude 0.50%

Figure 6

Hysteresis loops with different strain amplitudes and different cycles

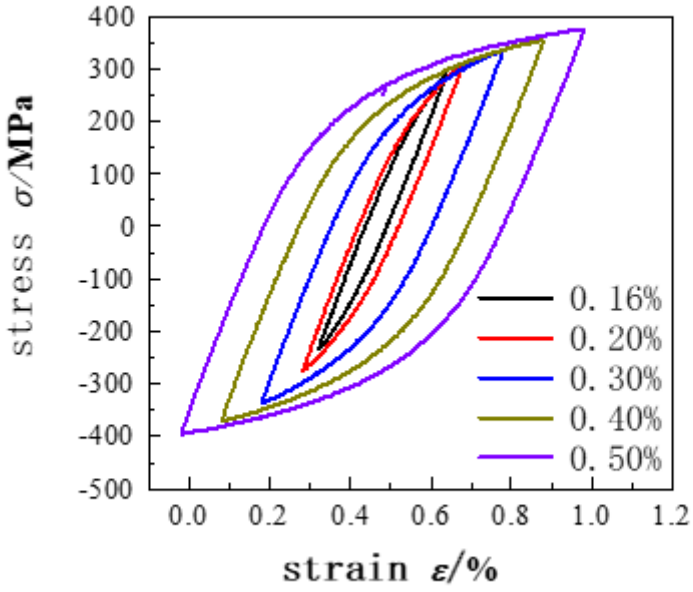

Figure 7

Hysteresis loops of cyclic loading at the 300 cycles under different strain amplitudes

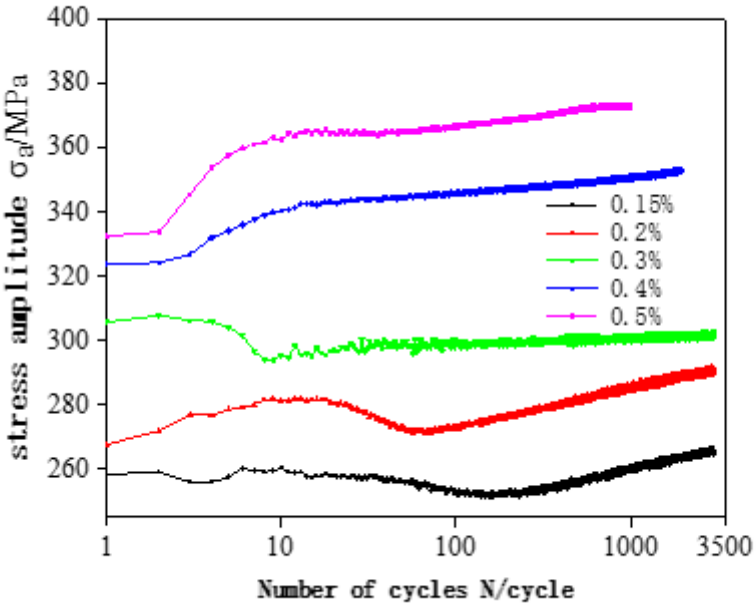

Figure 8

Curves of stress amplitude varying with the number of cycles at different strain amplitudes

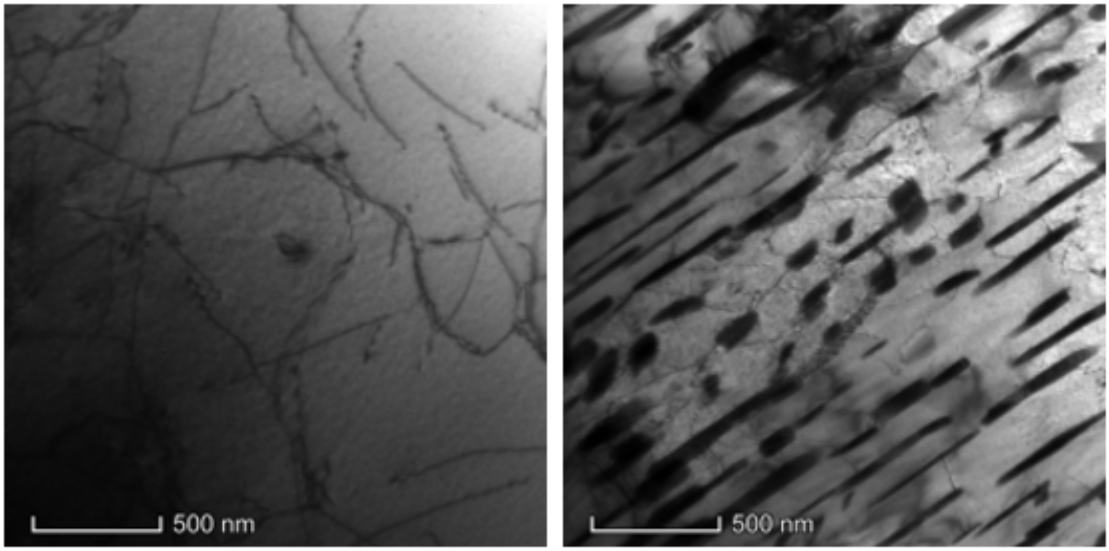

（a）Dislocation structure in ferrite　　（b）Dislocation structure in pearlite

Figure 9

Dislocation structure in the original sample

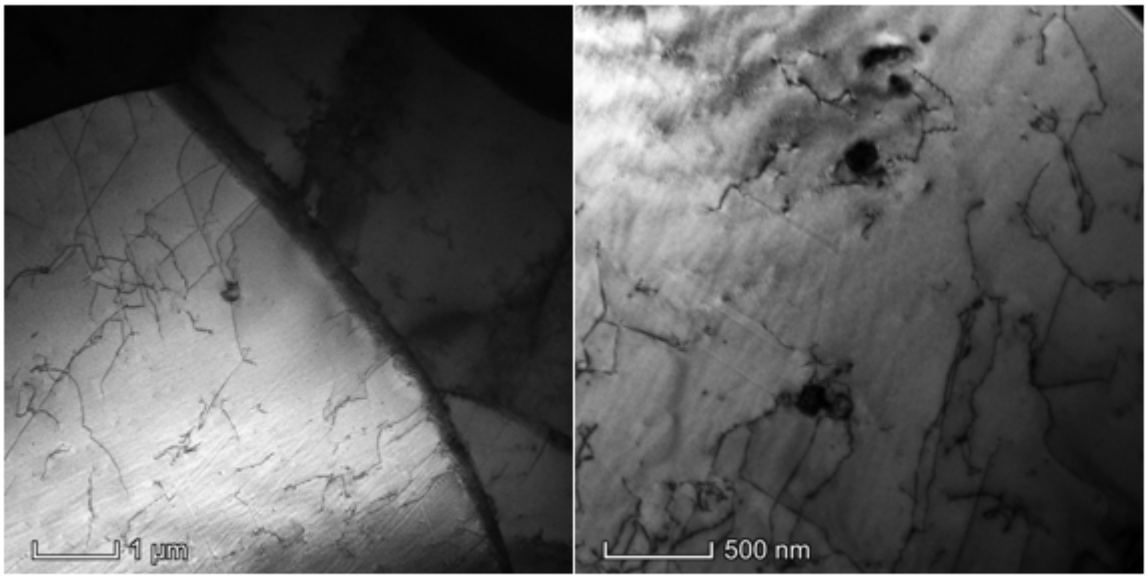

(a)Dislocations at grain boundaries (b)pinning of dislocations by cementite

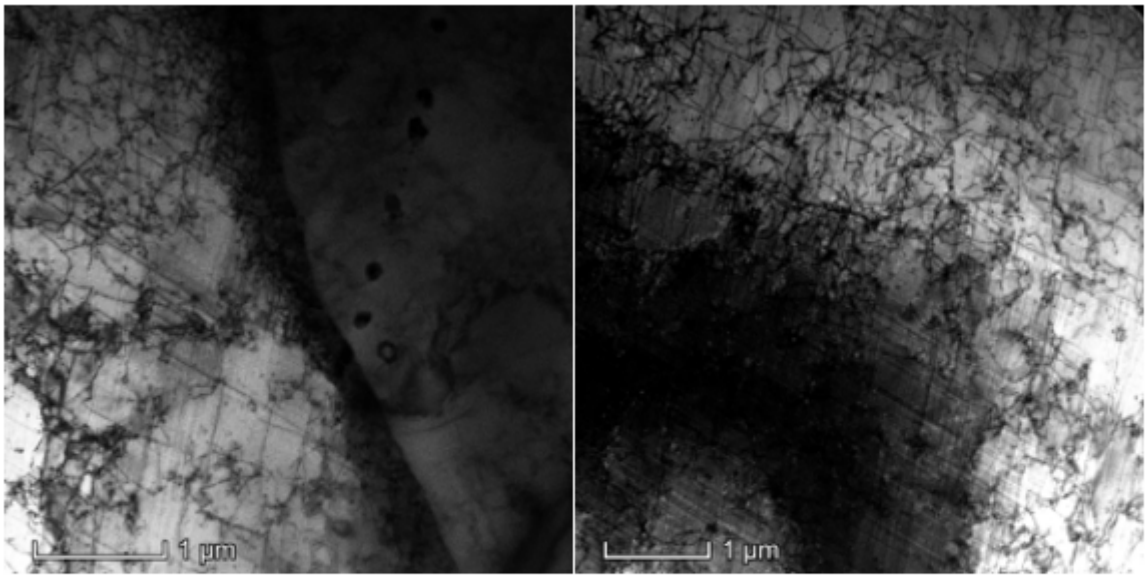

(c)Dislocation stacking product at grain boundaries (d)dislocation entanglement

Figure 10

Dislocation structure with 0.2% strain amplitude cycling for 10 cycles

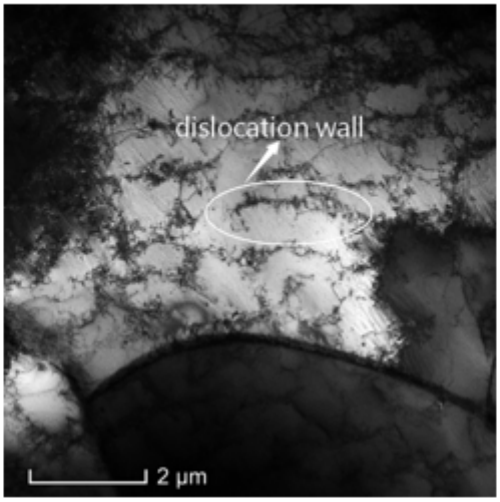

(a) Dislocation structure in ferrite

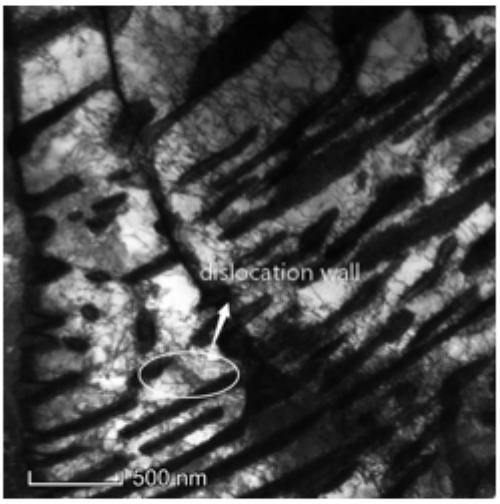

(b)Dislocation structure in pearlite

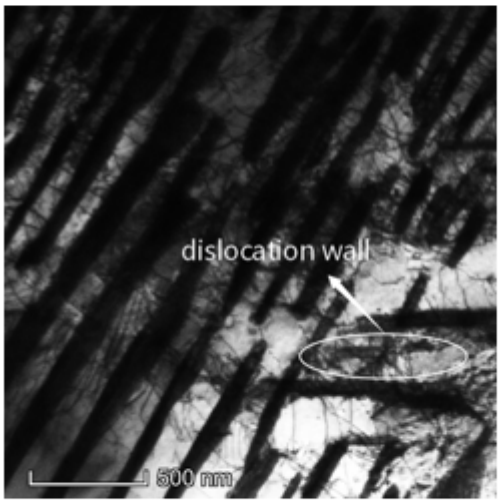

(c)Dislocation wall in pearlite

Figure 11

Dislocation structure with 0.2% strain amplitude cycling for 60 cycles

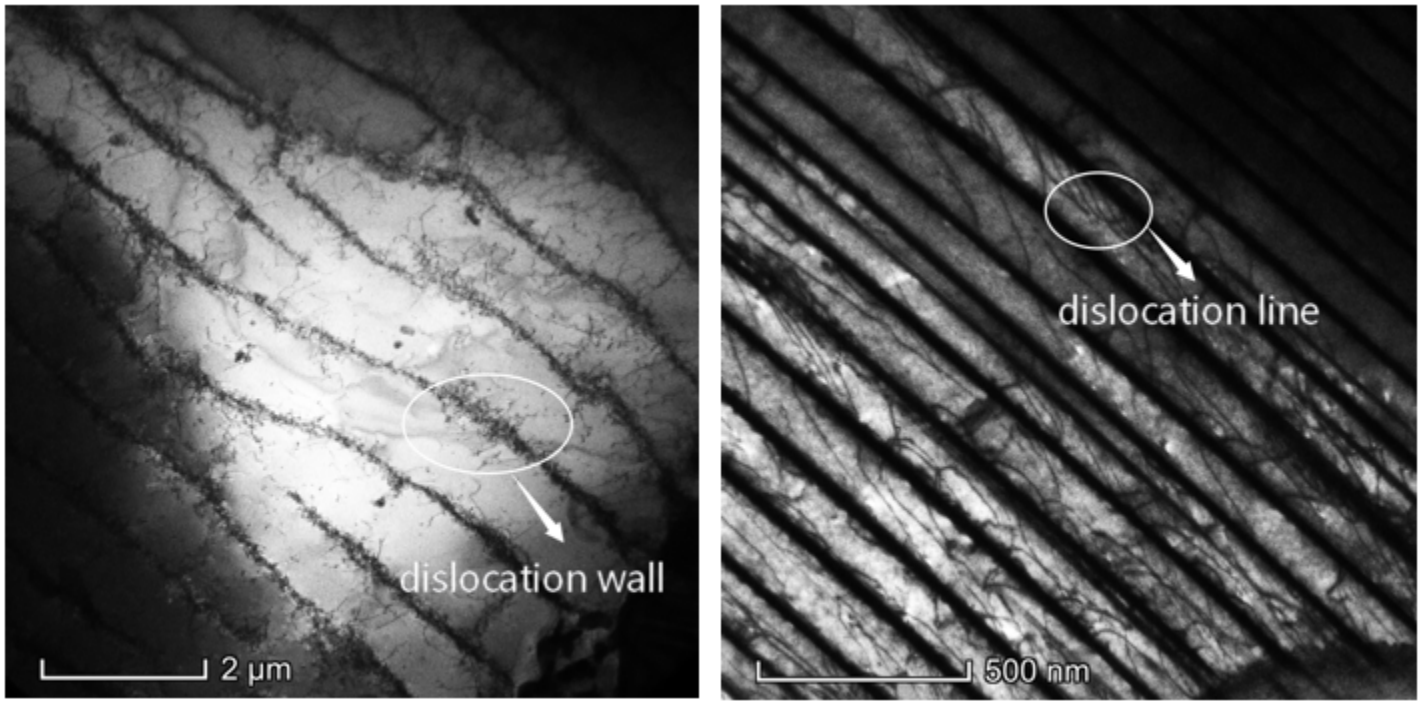

（a）Dislocation structure in ferrite　　（b）Dislocation structure in pearlite

Figure 12

Dislocation structure with 0.2% strain amplitude cycling for 3000 cycles

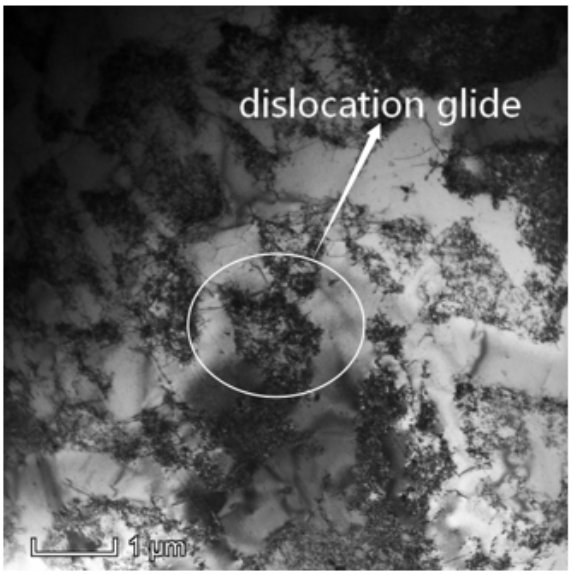

（a）The strain amplitude 0.16% and the cycle is 3000 cycles

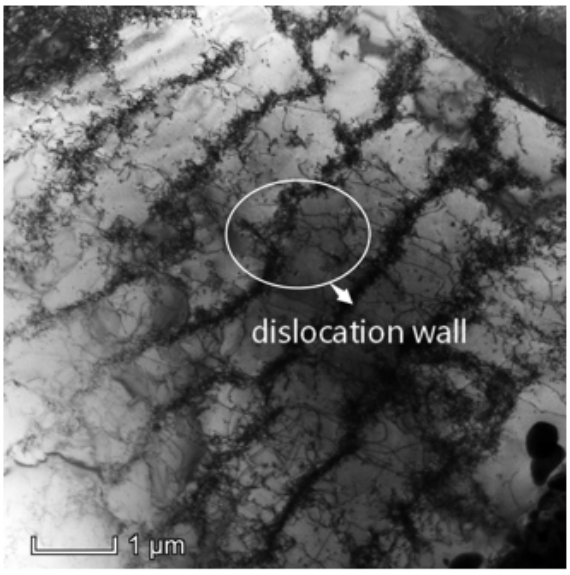

（b）The strain amplitude 0.30% and the cycle is 3000 cycles

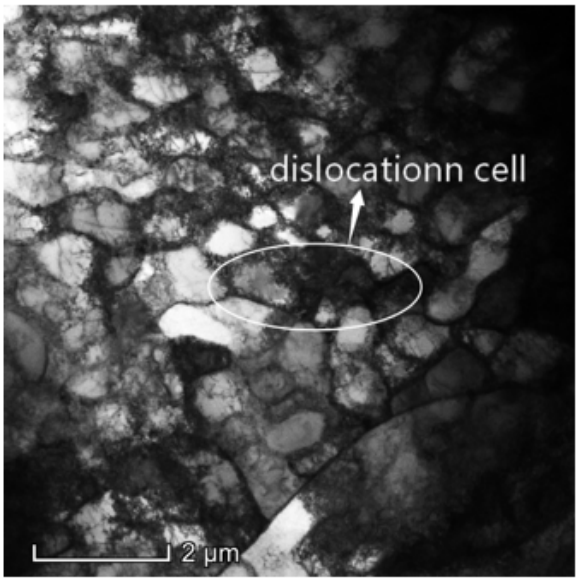

（c）The strain amplitude 0.40% and the cycle is 2454 cycles

Figure 13

Dislocation structures in ferrite with different cyclic orders under different strain amplitudes

Supplementary Files

This is a list of supplementary files associated with this preprint. Click to download.

- Tab.1.xlsx
- Tab.2.xlsx
- Tab.3.xlsx